Journal of proteome research

pubs.acs.org/jpr

Article

Digital Microfluidics for Microproteomic Analysis of Minute Mammalian Tissue Samples Enabled by a Photocleavable Surfactant

Calvin Chan, Jiaxi Peng, Vigneshwar Rajesh, Erica Y. Scott, Alexandros A. Sklavounos, Maryam Faiz, and Aaron R. Wheeler*

Cite This: *J. Proteome Res.* 2023, 22, 3242−3253

Read Online

ACCESS | Metrics & More | Article Recommendations | Supporting Information

ABSTRACT: Proteome profiles of precious tissue samples have great clinical potential for accelerating disease biomarker discovery and promoting novel strategies for early diagnosis and treatment. However, tiny clinical tissue samples are often difficult to handle and analyze with conventional proteomic methods. Automated digital microfluidic (DMF) workflows facilitate the manipulation of size-limited tissue samples. Here, we report the assessment of a DMF microproteomics workflow enabled by a photocleavable surfactant for proteomic analysis of minute tissue samples. The surfactant 4-hexylphenylazosulfonate (Azo) was found to facilitate fast droplet movement on DMF and enhance the proteomics analysis. Comparisons of Azo and *n*-Dodecyl *β*-D-maltoside (DDM) using small samples of HeLa digest standards and MCF-7 cell digests revealed distinct differences at the peptide level despite similar results at the protein level. The DMF microproteomics workflow was applied for the sample preparation of ∼3 *μ*g biopsies from murine brain tissue. A total of 1969 proteins were identified in three samples, including established neural biomarkers and proteins related to synaptic signaling. Going forward, we propose that the Azo-enabled DMF workflow has the potential to advance the practical clinical application of DMF for the analysis of size-limited tissue samples.

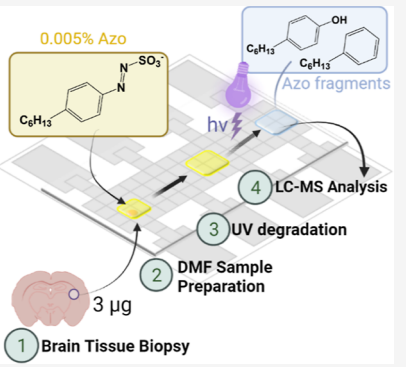

KEYWORDS: *digital microfluidics, photocleavable surfactant, tissue microproteomics, sample preparation*

INTRODUCTION

Tissue samples can provide great clinical value in advancing biological understanding of a disease.[1,2] In particular, global proteome profiling of tissue samples has emerged as a promising technique for disease biomarker discovery and the development of novel strategies for early diagnosis and treatment.[3,4] However, clinical tissue samples are often limited in size and challenging to handle, requiring substantial manual dexterity and labor to process them using standard tools (such as tweezers, pipet tips, and tubes). Conventional proteomic analysis methods typically require tissue samples greater than 1 mg in size,[5] while microproteomic analysis of smaller samples have less consistent results.[6] As such, specialized workflows are required to analyze minute tissue samples.[7]

Microfluidic technologies provide miniaturization of sample preparation workflows for minute samples.[8−10] In particular, digital microfluidics (DMF) has emerged as a valuable tool for handling and processing size-limited tissue samples.[11−13] DMF enables programmable control of the fluid movement across an open array of electrodes. This format has proven to be useful for the extraction of analytes from tissue samples into droplets of organic solvent with no risk of clogging, which is a critical challenge for systems relying on microchannels.[14] Previously, the capability of DMF for rapid tissue-liquid extraction was demonstrated by using milligram-sized core needle biopsy samples. In these studies, biopsy tissue samples were sandwiched between top and bottom DMF plates to allow extraction of steroid hormone analytes followed by quantification by liquid chromatography tandem mass spectrometry[12] (LC-MS/MS) or on-chip immunoassays[13] to monitor the progression of breast cancer.

Digital microfluidics has also been touted as a technique useful for microvolume proteome sample processing, including a recent report of an end-to-end-automated proteome processing pipeline.[15] DMF has some advantages for this application (including automation without robotics) and also has some disadvantages (low throughput relative to robotic workstations); it is always important to consider carefully which technology is best suited to a particular application. Among many proof-of-concept reports of DMF for proteomics, DMF has typically been applied to process presolubilized protein-containing samples (a notable counterexample is the recent, pioneering report[16] of a technique to extract and process proteomes from single *C. elegans*). Here, we sought to explore whether DMF was appropriate for on-chip extraction

Received: May 9, 2023
Published: August 31, 2023

of proteins from microtissue biopsies, because to our knowledge, this is the first example of using DMF for this application.

A critical challenge in this work was to identify a surfactant that (on the one hand) was compatible with protein extraction and LC-MS analysis, while (on the other hand) being able to support droplet manipulation on DMF devices (noting that there is extensive literature[17−19] about surfactants that provide the necessary combination of viscosity, surface tension, and resistance to protein fouling that is required for DMF). Specifically, the conventional surfactants that are used in DMF, such as poloxamers[17,18] and poloxamines,[19] are thought to be incompatible with LC-MS analysis, and the steps required to remove them can result in substantial analyte losses. In recent reports,[15,16,20−23] this challenge has been addressed by using sugar-derivative surfactants, such as *n*-dodecyl-*β*-D-maltoside (DDM), or 3-dodecyloxypropyl-1-*β*-D-maltopyranoside (DDOPM), which elute late in the LC gradient. Although these sugar derivatives are compatible with both DMF and LC-MS, their tendency to cause diminished droplet velocities on DMF is a known limitation.[15] Here we report a new strategy to address the challenge of DMF- and LC-MS-compatibility: the use of photocleavable surfactants. In particular, 4-hexylphenylazosulfonate (known in shorthand as "Azo") has recently become popular for LC-MS methodologies, as it provides solubility properties that are useful for sample processing and also can be degraded into alkylphenol and alkylbenzene residues upon ultraviolet irradiation,[24] so that it does not interfere with analysis by LC-MS. Azo has recently been shown to enhance enzymatic digestion kinetics for the ultrafast bottom-up proteomics sample preparation of membrane proteins,[25] extracellular matrix proteins,[26] small sections of cardiac tissue,[27] and exosomes.[28] We hypothesized that Azo might also be useful for DMF; to the best of our knowledge, this is the first report of the use of Azo or any other UV-cleavable surfactants with DMF.

Here, we report the use of Azo for DMF proteome sample processing with and without photocleavage. First, the performance of Azo was evaluated for microproteomic protein extraction and sample preparation on DMF, demonstrating distinct differences relative to DDM. Then, we applied this workflow for the extraction and proteome profiling of 2 mm diameter biopsy punched murine brain tissues. A total of 1969 proteins were identified from the analysis of punched tissue samples, covering a wide range of biological functions. We propose that this workflow is an important first step for an automated, fast, and sensitive microprotomics analysis of size-limited clinical tissue samples on DMF.

MATERIALS AND METHODS

Chemicals and Reagents

Cell media reagents, acetonitrile (ACN), formic acid (FA), water (LC/MS-grade), and Pierce HeLa protein digest standard were purchased from Thermo Fisher Scientific (Waltham, MA, USA). 0.5% w/w Azo in 25 mM aqueous ammonium bicarbonate, *n*-dodecyl-*β*-D-Maltoside (DDM), tris(2-carboxyethyl)phosphine (TCEP), iodoacetamide (IAA), triethylammonium bicarbonate (TEAB), and trypsin were obtained from Sigma-Aldrich (Oakville, ON, CA). Lys-C was purchased from Promega (Madison, WI, USA).

Cell Culture and Cell Samples

MCF-7 cells were grown in Dulbecco's modified Eagle's medium (DMEM) with 10% fetal bovine serum, penicillin (100 U/mL), and streptomycin (100 μg/mL) in T-25 culture flasks in a humidified incubator with 5% CO_2 at 37 °C. Cells were trypsinized, washed with phosphate-buffered saline (PBS) three times (each time centrifuging at 300*g*, 5 min), and then suspended in PBS at densities ranging from 50,000 to 100,000 cells/mL (determined via hemacytometer). One microliter samples (about 50−100 cells) were aliquoted into tubes and stored at −80 °C until analysis.

Mouse Tissue Samples

8−10-week-old male C57/Bl6 mice purchased from Charles River were treated according to protocols (20012650) approved by the Animal Care Committee at the Division of Comparative Medicine of the University of Toronto. Their brains were removed and flash-frozen in liquid-nitrogen-cooled isopentane and stored at −80 °C until use. The tissues were biopsied with a 2-mm biopsy punch (Thermo Fisher Scientific). Ten-micrometer-thick tissue sections were cut using a cryostat (NX-70, Thermo Fisher Scientific), mounted on Ephredia Shandon multispot slides (Thermo Fisher Scientific), and stored at −80 °C until use.

DMF Device Fabrication and Control

DMF devices comprising (i) bottom plates bearing 68 roughly square (2.2 × 2.2 mm) chromium driving electrodes (where 60 of them formed a 4 row ×15 column electrode array) and 12 reservoir electrodes, and (ii) top plates bearing an indium−tin oxide counterelectrode were fabricated as described previously.[29] Top plates and bottom plates were assembled with ∼190-μm-thick interplate spacers formed from two-ply pieces of Scotch double-sided tape (3 M). This spacer defines "unit droplets" (with volume sufficient to cover a single driving electrode) of approximately 0.9 μL. The devices were controlled and droplet movements were programmed by an open-source DropBot V3 system (Sci-Bots Inc., Toronto, ON). These were interfaced with the DropBot through a pogo-pin connector, and the electrodes were actuated in preprogrammed steps, which allowed droplet dispensing, moving, and mixing by (typically) applying 100 V_{RMS} as square waves at 10 kHz (parameters optimized as described below).

Surfactant Concentration Optimization

Azo was diluted in aqueous solution of tetraethylammonium bicarbonate (TEAB, 50 mM) to prepare solution with final Azo concentrations ranging from 0.0005% to 0.1% w/w Using a modified version of a method described previously,[30] force−velocity curves were generated to identify optimal working conditions. Briefly, double-unit droplets were dispensed onto the electrode array on DMF devices and shuttled back and forth between adjacent electrodes. Velocity was monitored as a function of driving force, and each condition was repeated in triplicate. In subsequent experiments, a 100 V_{RMS} driving voltage was used (corresponding to ∼30 μN/mm).

Photodegredation of Azo

Azo-containing samples were photodegraded by lighting a Mixjoy 125 W mercury vapor light bulb (Sylstar, Chino, CA, USA) in a 120 V Catalina desk lamp (Evolution Lighting LLC, Pembroke Pines, FL, USA) positioned 10 cm away from the sample. In initial experiments, 20 μL aliquots of Azo (0.05% or 0.005% w/w in 50 mM TEAB) in polypropylene centrifuge

https://doi.org/10.1021/acs.jproteome.3c00281
J. Proteome Res. 2023, 22, 3242−3253

tubes (Axygen) were irradiated on ice for up to 40 min. At regular intervals, 2 μL aliquots were removed for absorbance analysis (190−850 nm with autorange path length enabled) using a NanoDrop One spectrometer (Thermo Fisher Scientific). For all other experiments, sample volumes, irradiation times, and other conditions are indicated in the subsections below.

Protein Standard Digest Analysis

Protein standard solutions (containing albumin, catalase, cadherin, haptoglobin, or serotransferrin) were prepared by dissolving 1 mg of each protein in 1 mL of deionized (DI) water. Each solution was then diluted and mixed to 10 ng/μL (of each protein) in either (a) 0.005% w/w Azo in 50 mM aqueous TEAB or (b) only 50 mM aqueous TEAB as control. Aliquots (1 μL) of protein standard mixtures were mixed with 1 μL of 20 mM TCEP in 50 mM TEAB in tubes and then incubated for 10 min at 70 °C in a thermocycler (Bio-Rad). Aliquots (1 μL) of 50 mM IAA in 50 mM TEAB were added to each tube, which was incubated for 30 min at room temperature. Aliquots (3 μL) of digestive enzyme mixture (10 ng/μL trypsin and 10 ng/μL LysC in 50 mM ammonium bicarbonate) were added to each tube and incubated at 37 °C overnight in a thermocycler. Aliquots (2 μL) of 0.5% v/v formic acid in water were then added to each tube to quench the digestions. Finally, Azo-containing samples were irradiated with UV light for 0.5, 1, 2, or 3 h on ice (as described above). The control protein mixture (without Azo) was not irradiated, and finally, 7 μL of each processed sample was pipetted into a 96-well plate (Eppendorf) for LC-MS analysis.

HeLa Protein Digest Standard Analysis

Standard surfactant solutions (0.005% w/w) were prepared by diluting 0.5% w/w Azo or DDM in 50 mM TEAB and concentrated formic acid (to a final concentration of 0.1%). A surfactant-free solution consisting of 0.1% formic acid in water was also prepared. HeLa protein digest standards were formed by dissolving lyophilized lysate at 2 ng/μL in standard Azo solvent, standard DDM solvent, or a solution of aqueous 50 mM TEAB. In typical analyses, 5 μL of each sample was injected into the LC-MS in triplicate.

Proteomic Sample Preparation of MCF-7 Cells in Tube

Aliquots (1 μL) of samples containing 50−100 suspended MCF-7 cells were thawed and then mixed with 1 μL of 20 mM TCEP in 50 mM TEAB and 1 μL of (1) 0.05% w/w Azo in 50 mM TEAB, (2) 0.05% w/w DDM in 50 mM TEAB, or (3) 50 mM TEAB as a control. Samples were then incubated for 10 min at 70 °C in a thermocycler (Bio-Rad). Aliquots (1 μL) of 50 mM IAA in 50 mM TEAB were added to each tube, which was incubated for 30 min at room temperature. Aliquots (3 μL) of the digestive enzyme mixture (10 ng/μL trypsin and 10 ng/μL LysC in 50 mM ammonium bicarbonate) were added to each tube, which were incubated at 37 °C for 3 h in a thermocycler. Aliquots (2 μL) of 0.5% v/v formic acid in water were then added to each tube to quench the digestions, and azo-containing samples were irradiated with UV light for 10 min on ice. Finally, 7 μL of each processed sample was pipetted into a 96-well plate (Eppendorf) for LC-MS analysis.

Proteomic Sample Processing of Tissue Samples on DMF

Reagents were dissolved in 0.005% w/w Azo in 50 mM TEAB unless otherwise stated. Frozen tissue punch samples (2-mm-diameter circles with 10-μm thickness) were thawed and suspended in 5 μL of 0.005% w/w Azo in 50 mM TEAB. Each 5 μL droplet was then flash-frozen by exposing it to dry ice and transferring it to a 200-μL microcentrifuge tube (Axygen), where it was allowed to thaw again. One microliter of 100 mM TCEP was added to each sample, and the tissue mixture was pipetted 10 times to dissociate the tissues. Each sample was then incubated for 10 min in a thermocycler (Bio-Rad) at 70 °C. Three dissociated tissue samples were loaded on to a DMF device (positioning each onto a bottom plate by a pipet, followed by assembling it with a top plate) for parallel processing, and then the device was interfaced with the DropBot. A solution of 100 mM IAA was loaded into a reservoir, and three single-unit droplets were dispensed onto the array. Each IAA droplet was merged with a sample droplet, followed by incubating it at room temperature for 30 min. Digestive enzyme mixture solution (10 ng/μL trypsin and 10 ng/μL LysC) was loaded into a reservoir, three single-unit droplets were dispensed onto the array, and each was merged with a sample droplet. The DMF chip was then disconnected from the DropBot and wrapped in a parafilm before incubating at 37 °C for 4 h in an incubator. After extraction from the incubator, unwrapping, and reconnecting the device to the DropBot, 1% v/v formic acid with 0.005% w/w Azo in DI water was loaded into a reservoir, and three single-unit droplets were dispensed onto the array, where each was merged with one of the samples. Finally, the DMF chip was placed on ice and irradiated with UV light for 10 min. The top plate was then removed, and 6 μL of each sample was collected by pipet for transfer to a 96-well plate (Eppendorf) for LC-MS analysis.

HPLC-MS/MS Analysis

Experiments were performed on a Q Exactive HF-X mass spectrometer coupled to an EASY-nLC 1200 system (Thermo Fisher Scientific). Each sample was loaded by an autosampler onto a C18-trap column (3 cm, 100 μm i.d., Polymicro Technologies) at a flow rate of 2 μL/min. The sample was then eluted into a fused silica microcapillary column (12 cm, 100 μm i.d., Polymicro Technologies), packed with 1.9-μm-diameter reversed-phase C18 particles (ReproSil-Pur 120 Å, Dr. Maisch GmbH) in-house. Mobile phase A (water with 0.1% formic acid, v/v) and mobile phase B (80/20/0.1% ACN/water/formic acid, v/v/v) were used to generate a linear gradient of 3−30% B for 90 min, followed by a linear increase from 30 to 45% B for 20 min, then a linear increase from 45 to 95% B for 1 min and maintaining it at 95% B for 14 min. The flow rate was set as 300 nL/min. A full mass scan collected by the Orbitrap mass analyzer was from m/z 375 to 1575 with a resolution of 120,000, while the automatic gain control (AGC) target was 5×10^5 and the maximum injection time was 50 ms. Precursor ions with charges of +2 to +6 were fragmented by using high-energy collision with 27% normalized energy at a resolution of 60,000, AGC of 5×10^4, and a maximum injection time of 250 ms. Previously selected precursor ions were excluded from further sequencing for 20 s. The degraded Azo product was monitored with a full mass scan collected by the Orbitrap mass analyzer from m/z 50 to 400 with a resolution of 120,000, while the AGC target was 5×10^5 and the maximum injection time was 50 ms using the same high-performance liquid chromatography (HPLC) gradient.

Proteomic Data Analysis

Raw data files were evaluated by MaxQuant[31] (version 1.6.4.0). Data from HeLa and MCF-7 cells were searched against the Uniprot human protein database UP000005640 (accessed November 11, 2021) and potential contaminants. Data from

https://doi.org/10.1021/acs.jproteome.3c00281
J. Proteome Res. 2023, 22, 3242−3253

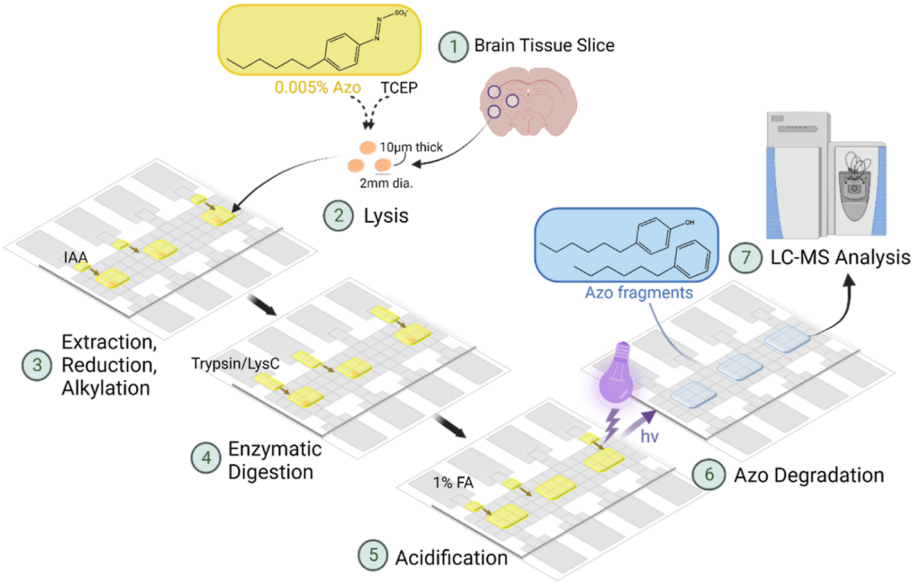

Figure 1. Schematic of miniaturized bottom-up proteomics workflow using Azo on digital microfluidics. (1) Tissue biopsy punches from mouse brain were transferred to tubes for (2) dissociation in 0.005% w/w Azo (yellow). The on-chip workflow includes (3) protein extraction, reduction with TCEP, and alkylation with IAA, (4) a 4-h protein digestion with trypsin and LysC, (5) quenching with formic acid, and (6) Azo degradation by exposure to UV irradiation before (7) HPLC-MS analysis.

mouse brain tissue were searched against the Uniprot mouse protein database UP000000589 (accessed December 26, 2019) and potential contaminants. Methionine oxidation and N-terminal protein acetylation were set as variable modifications, and cysteine carbamidomethylation was set as a fixed modification. Trypsin was set as specific proteolytic enzyme with a maximum of two missed cleavages for each peptide. The minimum peptide length was set to 6 or 7 amino acids for tissue samples and cell samples, respectively. The maximum peptide mass was set to 4600 Da. Both peptides and proteins were filtered with a maximum false discovery rate (FDR) of 0.01. The default settings of MaxQuant were used for all parameters not mentioned. Label-free quantification (LFQ) was performed by using classic normalization and a minimum ratio count of 2. Samples were evaluated in replicates, and "total" refers to all proteins identified from the pooled replicates, "average" refers to the average number per replicate, and "LFQ average" refers to the average number per replicate after applying the higher confidence threshold of the LFQ algorithm. In typical experiments, analysis of reagent blanks identified less than 20 protein groups, while in experiments with biological samples, hundreds or thousands of protein groups were identified. Finally, "protein intensity" is the MaxQuant value that correlates with the protein amount detected in the sample.

After MaxQuant processing, data were further filtered using Perseus[32] to exclude from analysis proteins identified as decoys, potential contaminants, or identified exclusively by one-site modification. Perseus was also used to estimate the protein copy number with histone-level normalization using default parameters of the protein ruler add-on[33] (after confirming that the trends in peptide and protein identifications observed between samples were not affected by this process). GRAVY scores were calculated using the Sequence Manipulation Suite.[34] Processed data were visualized with OriginLab.[35] ShinyGo[36] and Pathview[37] were used for cellular components and KEGG[38] pathway analysis. PANTHER v17.0,[39] REVIGO (using GO database from January 1, 2023),[40] and Cytoscape v3.9.1[41] were used for biological function analysis. Finally, all the data were deposited to the ProteomeXchange Consortium (http://proteomecentral.proteomexchange.org) via the PRIDE partner repository[42] with identifier PXD039844.

RESULTS AND DISCUSSION

Azo-Enabled Proteomic Sample Preparation on Digital Microfluidics

The primary goal of this project was to develop a DMF sample preparation workflow for processing tissue biopsy samples for proteome profiling. As a key part of this plan, we decided to explore the use of the photocleavable surfactant Azo, with the hypothesis that the intact form of the surfactant might be suitable for proteomic sample processing and DMF droplet actuation, and that the degraded form would be well-suited for analysis by HPLC-MS. The proposed workflow includes (1) extraction of protein from tissue, (2) reduction and alkylation of disulfide bonds, (3) enzymatic digestion of proteins, (4) photocleavage of Azo, and (5) downstream LC-MS analysis (Figure 1).

As the first step toward this goal, we evaluated the effects of Azo on DMF droplet manipulation and proteomic analysis. In these experiments, the results were benchmarked to DDM, a surfactant commonly employed for microproteomics[43,44] that has been used previously for DMF sample preparation.[15,20] The choice of surfactant is crucial in bottom-up proteomics, as some surfactants have the potential to improve protein solubility and reduce nonspecific adsorption,[45] yet many other surfactants interfere with LC-MS analysis.[46] Azo is especially promising, as its photodegradation products have lower masses than typical peptides, and thus it is believed to have minimal interference in HPLC-MS proteomic analyses. There have been a few studies with Azo previously (including a report indicating high extraction of peptides relative to DDM from tissue samples[24]), but the performance of Azo for

https://doi.org/10.1021/acs.jproteome.3c00281
J. Proteome Res. 2023, 22, 3242−3253

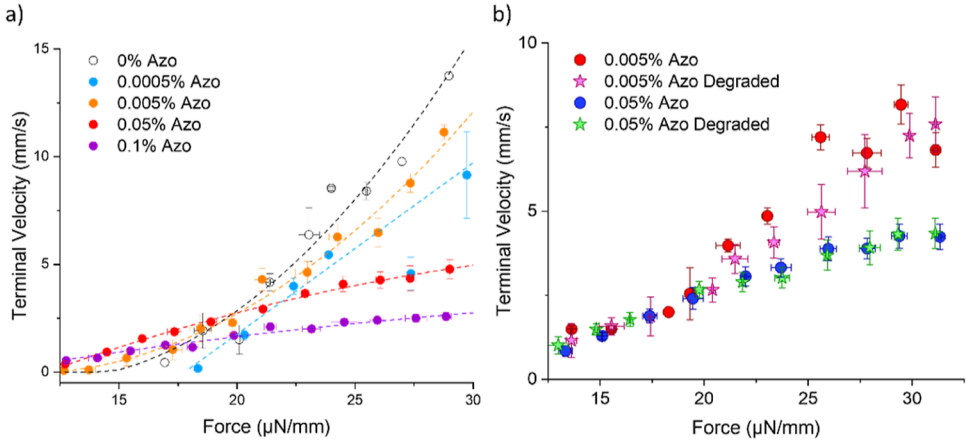

Figure 2. Evaluation of the mobility of droplets containing different concentrations of Azo on DMF before and after degradation. (a) Force−velocity plots for droplets containing Azo (0% w/w—black, 0.0005%—blue, 0.005%—orange, 0.05%—red, and 0.1%—purple), including curves to guide the eye. (b) Force−velocity curves for droplets before (circle) and after (star) UV degradation of Azo (0.005%—red circle and pink star, and 0.05%—blue circle and green star). Error bars are ±1 SD for n = 3 replicates per condition.

bottom-up proteomics relative to other surfactants is largely unexplored.

Optimization of Azo Concentration for Droplet Mobility on DMF

Droplet mobility on DMF depends on the surface tension and viscosity of the droplet solution.[30] The addition of surfactant affects both surface tension and viscosity, such that the choice of surfactant and its operating concentration are important decisions for optimal droplet movement on DMF. Furthermore, the addition of surfactants has been demonstrated to reduce nonspecific adsorption of biomolecules to the DMF surface, which improves the longevity of the DMF operation.[17−19] Until now, only two LC-MS compatible surfactants, DDM and DDOPM (both sugar derivatives), have been applied for proteomics sample preparation on DMF, and both have exhibited reduced droplet velocity compared to conventional DMF surfactants.[15,22] We speculated that Azo, which is a relatively small molecule relative to DDM and DDOPM, might support a greater droplet velocity in DMF operations.

Force−velocity curves[30] were generated to quantify droplet mobility for four concentrations of Azo (0.0005, 0.005, 0.05%, and 0.1% in 50 mM TEAB) with comparison to buffer alone (0% Azo in 50 mM TEAB). As expected and as shown in Figure 2a and Movie S1, lower concentrations of Azo support faster droplet mobility on DMF, but require increased threshold forces to initiate droplet movement.[30] Unexpectedly, the lowest tested concentration of Azo (0.0005%) seems to have a lower velocity than the second lowest concentration (0.005%) at some driving forces. We attribute this unexpected deviation to the poor reproducibility of droplet movement for 0.0005% Azo demonstrated by the large variance at forces greater than 25 μN/mm. With this in mind, we decided to adopt 0.005% Azo for the remaining experiments reported here (chosen purely on the basis of these DMF mobility experiments) and observed similar DMF performance in proteomic experiments (described below). Importantly, the velocity of 0.005% Azo is approximately three times faster than the velocity of DDM-containing droplets of the corresponding concentration[15] in the working regime of 20−30 μN/mm force. The high velocity of Azo is promising for efficient sample preparation on DMF.

Since Azo is designed to degrade upon exposure to UV irradiation, we decided to test the droplet velocities on DMF before and after photocleavage. As a first step, we evaluated the kinetics of the photocleavage reaction. As shown in Figure S1, tracking the absorbance of the −N═N− azo bond of the alkylbenzene-azosulfonate at 305 nm over time reveals that 10 min of irradiation (under the conditions used here) is sufficient for complete photocleavage of the diazo functionality, and thus, this duration was adopted for the remaining experiments described here. Figure 2b shows the DMF force−velocity curves for Azo before and after photocleavage. As shown, the reaction has little-to-no effect on DMF mobility, likely because degradation causes minimal change in droplet surface tension before and after photocleavage at low concentrations of Azo.[47]

Finally, we note that the output of the UV lamp used in this study is not a perfect spectral fit for Azo, and the vessels used in these experiments (plastic tubes and coated-glass devices) might be expected to reduce transmission of the low wavelengths that are optimal for Azo degradation. This suggests room for future studies into the efficiencies of different irradiation systems for methods relying on Azo. The question of efficiency is likely to be a tricky one as the system must be capable of degrading the Azo without causing photodamage to peptides in the sample. In preliminary studies carried out with a standard mixture of peptides irradiated under these conditions for 0, 0.5, 1.0, 2.0, or 3.0 h, no effects on peptide mass were observed (Table S1), which is consistent with previous reports using different irradiation conditions.[24]

Comparison of Azo and DDM for Microproteomics

Although both Azo and DDM are both known to be LC-MS-compatible surfactants, they have very different physicochemical properties that may result in the differences in the extraction/solubilization of peptides and/or how they separate in chromatography. For example, Azo is a photocleavable surfactant that degrades into nonamphiphilic alkylphenol and alkylbenzene residues, with molecular masses below the m/z window used in proteomics analysis. We were curious about the retention behavior of the degradation products and thus scanned a lower m/z window to be able to observe them in the chromatogram. As shown in Figure S2, the major hexylphenol degradation product (detected as hexylphenol and methylphenol—formed by in-source fragmentation) elutes at 83 min

https://doi.org/10.1021/acs.jproteome.3c00281
J. Proteome Res. 2023, 22, 3242−3253

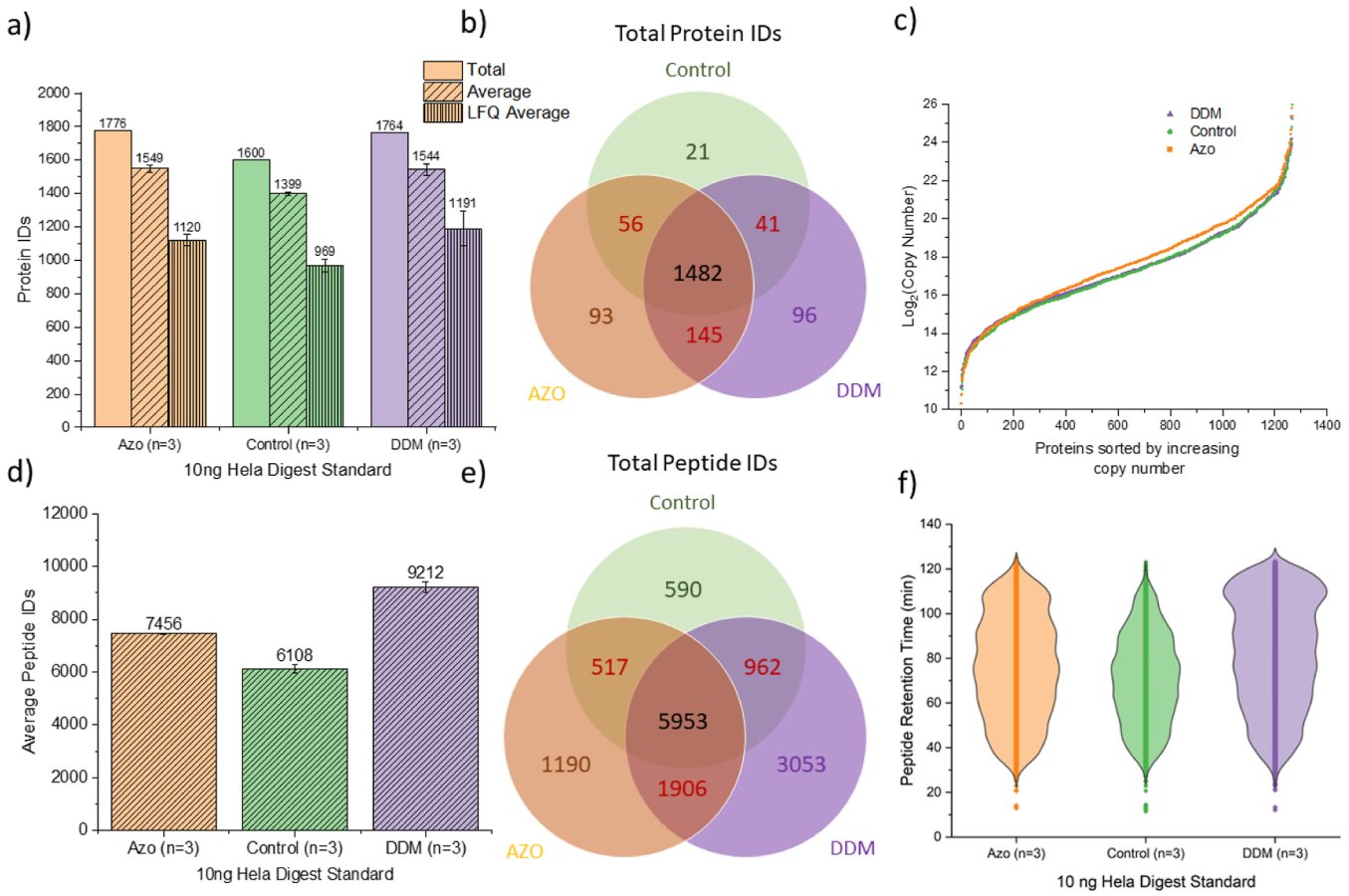

Figure 3. Proteomic analysis of 10 ng of HeLa digest standard in 0.005% w/w Azo (orange), 50 mM TEAB as the control (green), and 0.005% w/w DDM (purple). (a) Plot of total (open bars), average (diagonal cross-hatched bars), and LFQ average (vertical cross-hatched bars) proteins identified and (b) Venn diagram of total proteins identified. (c) Distribution of calculated protein copy numbers (from MaxQuant intensity) sorted by increasing copy number for proteins identified in all conditions. Note that the DDM data is largely hidden "behind" the control data. (d) Plot of average numbers and (e) Venn diagram of total peptides identified. (f) Violin plot of retention time distribution of identified peptides. Error bars for relevant data are ±1 SD for n = 3 replicates per condition.

in the RP-HPLC gradient used here. The low intensity and narrow elution of this product suggest that it has minimal effect on peptide detection. As far as we are aware, this is the first report of the chromatographic behavior of Azo degradation products in the context of a proteomic analysis.

In contrast to Azo, DDM remains intact, with a mass that overlaps with that of typical peptides detected in proteomic analysis. Further, it is relatively hydrophobic, and is known to elute at the end of the typical RP-HPLC gradients that are used in proteomic analysis.[48,49] This result was verified as shown in Figure S3, a broad elution of DDM monomers and dimers (with similar mass as peptides) is observed within typical proteomic mass windows late in the elution (around minute 125 in the gradient used here) from samples with relatively low concentration (0.005%) of DDM in blanks as well as in 10 ng of HeLa protein digest. Notably, trace DDM, likely carryover from prior samples, is sometimes observed in samples without DDM, which may affect the stability of peptide separation in future samples.

We compared the performance of Azo and DDM through the LC-MS analysis of 10 ng of samples of HeLa protein digest standard dissolved in 0.005% Azo, 0.005% DDM, or 50 mM TEAB as a control. A summary of the protein identifications (Figure 3a,b) demonstrates that the addition of either Azo or DDM increases protein identifications compared to when no surfactant is used, likely because of improved peptide solubilization and reduced sample loss to nonspecific adsorption to surfaces. Protein intensity was normalized to histone levels using the proteome ruler[33] to estimate protein copy number, and as shown in Figure 3c, the majority of proteins identified in Azo-containing HeLa digest standard samples are detected with more copies than in DDM-containing samples and controls. In contrast, the addition of DDM allows for many more identified peptides than the addition of Azo or control (Figure 3d,e), which, interestingly, did not have observable differences at the protein identification level (Figure 3a). In reviewing the identifications, this observation is explained by the fact that the extra peptides identified in the DDM group were largely to proteins that were already identified by other peptides. Finally, we investigated the differences in peptide identification by examining the retention time distribution shown in Figure 3f. The retention time distributions of peptides in both Azo and DDM were similar, except for a group of peptides eluting near the end of the gradient for DDM.

The differences in peptide identification for the two surfactants were explored in detail. As shown in Figure S4, the addition of DDM allows for the identification of more peptides of high molecular weight and higher charge state, many of which elute after 80 min. In contrast, the addition of

https://doi.org/10.1021/acs.jproteome.3c00281
J. Proteome Res. 2023, 22, 3242−3253

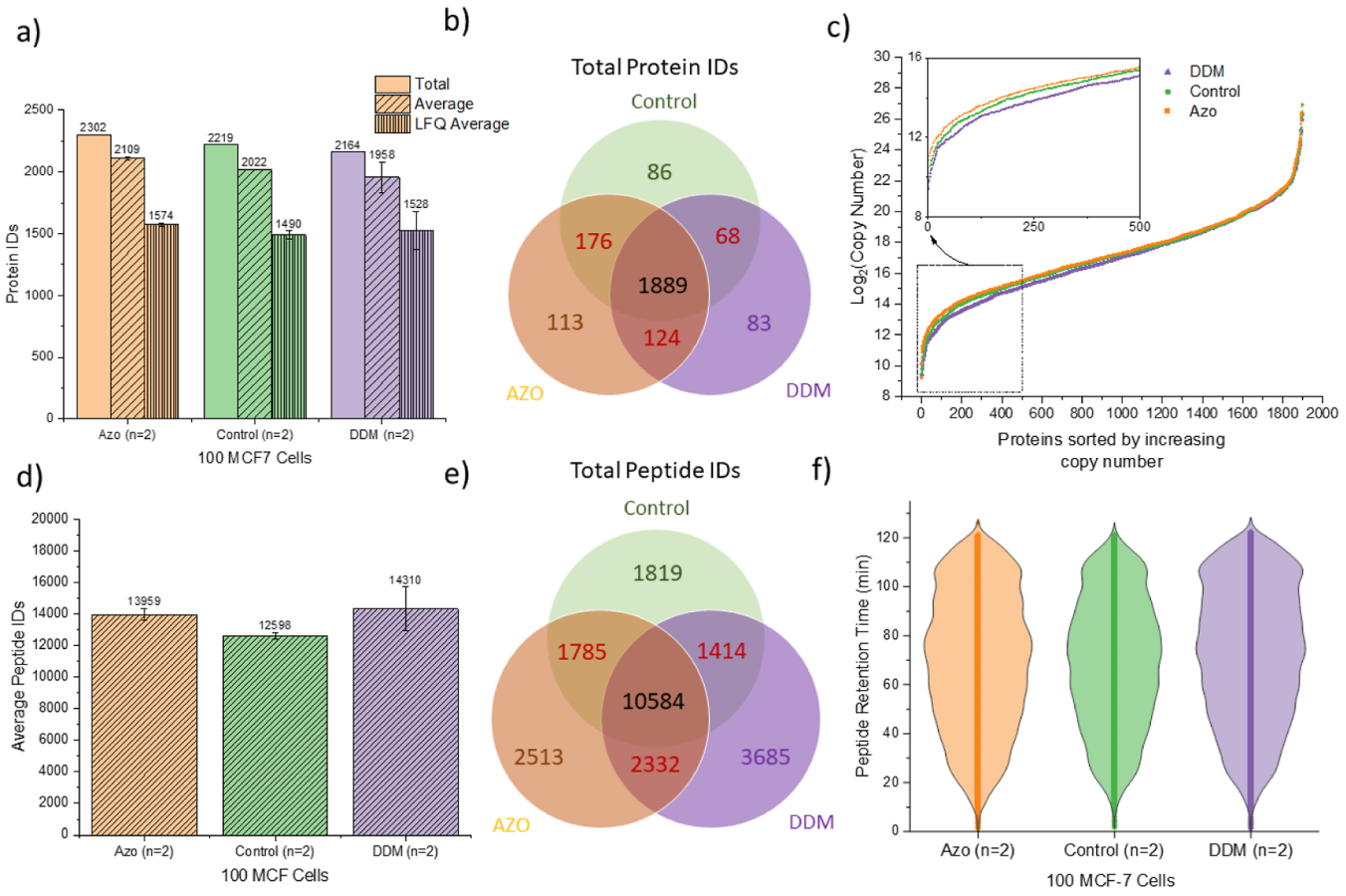

Figure 4. Proteomic analysis of samples containing 50−100 MCF-7 cells extracted with 0.005% w/w Azo (orange), 50 mM TEAB as control (green), and 0.005% w/w DDM (purple). (a) Plot of total (open bars), average (diagonal cross-hatched bars), and LFQ average (vertical cross-hatched bars) proteins identified and (b) Venn diagram of total proteins identified. (c) Distribution of calculated protein copy numbers (from MaxQuant intensity) sorted by increasing the copy number for proteins identified in all conditions. The inset is a magnified view of the distribution for the 500 proteins detected with lowest copy number. (d) Plot of average number and (e) Venn diagram of total peptide identifications. (f) Violin plot of retention time distribution of identified peptides. Error bars are ±1 SD for n = 2 replicates per condition.

Azo allows for the detection of more peptides of low molecular weight with lower charge states, many of which elute earlier than 70 min. Although a well-digested HeLa standard was used in this comparison, we examined the proportion of missed cleavages to confirm that the larger and highly retained peptides did not correspond to a large proportion of incompletely digested peptides. We hypothesize that the relatively late elution and identification of peptides in samples containing DDM are associated with the prolonged retention of DDM on the column which promotes the elution of highly hydrophobic peptides. Although not studied here, it may be useful to explore using both Azo and DDM in the future to potentially increase the numbers of peptides identified further.

To evaluate the effects of Azo and DDM in the analysis of other sample types (as well as those containing low amounts of protein), we digested samples containing 50−100 MCF-7 cells in 0.005% Azo, 0.005% DDM, or buffer for proteomic analysis. The summary of protein identifications (Figure 4a,b) shows that the addition of Azo results in slightly more protein identifications with a higher proportion of unique proteins. Interestingly, the DDM-containing sample and the surfactant-free control have similar results at the protein level for this sample type, suggesting that DDM does not confer much of an advantage in the extraction process relative to control. As indicated above, protein copies were estimated by normalizing protein intensities to histone protein intensities to account for differences in sample loading (Figure 4c). Although the difference is less obvious in this sample compared with the HeLa cell digest standard, the proteins identified in Azo samples were observed at higher copy numbers, especially at lower protein abundance (Figure 4c inset). This observation is promising for size-limited samples that contain lower total protein numbers than conventional samples. Like the HeLa digest standard results, the summary of peptide identifications (Figure 4d,e) shows that the greatest number of peptides can be identified uniquely in DDM-containing samples and that both Azo and DDM samples outperform the surfactant-free control for peptide identifications. The distribution of peptide retention time (Figure 4f) also shows more peptides elute later (after 100 min) in DDM samples compared to Azo samples or control, though the effect is less prominent compared to the retention time profile of DDM with the HeLa digest standard.

Further investigation of peptides identified from digested MCF-7 cells yielded results similar to those from the HeLa digest standard, as shown in Figure S5. DDM-containing samples are enriched in late-eluting, larger peptides with higher charge state, whereas Azo-containing samples favor earlier elution of smaller peptides with lower charge state. The proportion of missed cleavages is comparable across all three conditions; however, the ability of DDM to enable detection of

https://doi.org/10.1021/acs.jproteome.3c00281
J. Proteome Res. 2023, 22, 3242−3253

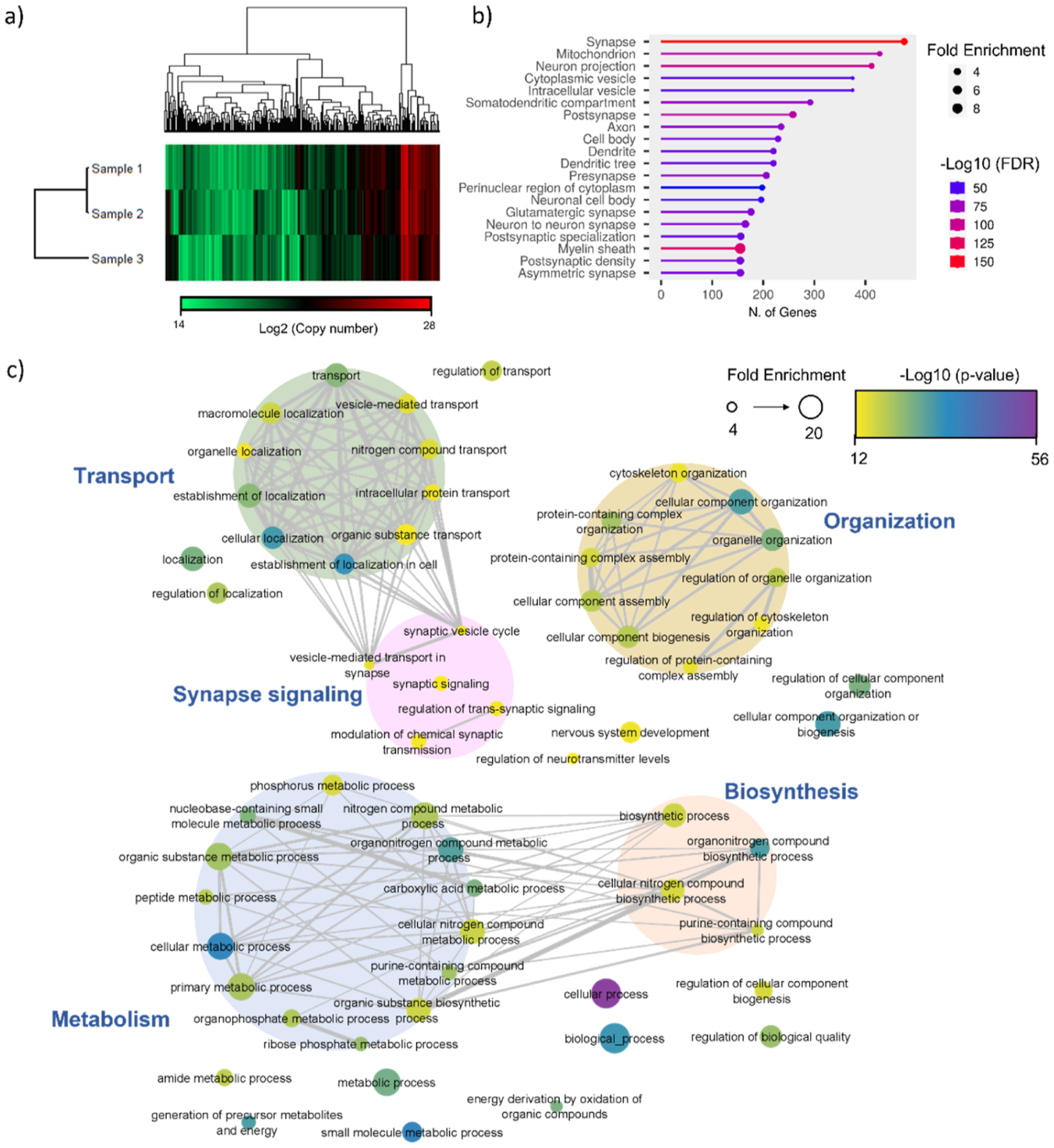

Figure 5. Proteomic analysis of murine brain biopsies using the automated DMF workflow with 0.005% w/w Azo. (a) Heat map of protein copy number (green = low; red = high) for 1969 identified protein groups (columns, with hierarchical clustering) in three samples (rows). (b) List of numbers of protein groups categorized as a function of the most common 20 cellular components found in the samples. Marker size indicates frequency of the gene-ontology (GO) term in the gene-ontology annotation (GOA) database relative to all protein-coding genes, and marker color (red = high confidence, blue = low confidence) indicates Log_{10}(FDR) corresponding to statistical confidence of protein assignment. (c) Graphical representation of the top 100 biological process that were associated with the identified protein groups. Marker size indicates frequency of the GO term in the underlying GOA database relative to all protein-coding genes, marker color (ranging from purple = high confidence to yellow = low confidence) indicates the -Log_{10}(p-value) corresponding to statistical confidence of protein function assignment, and gray lines indicate the correlation between biological functions.

more long peptides may explain the slightly higher proportion of detected peptides with missed cleavages compared to the other two conditions. Despite the increased detection of longer peptides in DDM-containing samples, 42% of the proteins detected in both the conditions have equal or higher sequence coverage in the Azo-containing sample.

https://doi.org/10.1021/acs.jproteome.3c00281
J. Proteome Res. 2023, 22, 3242−3253

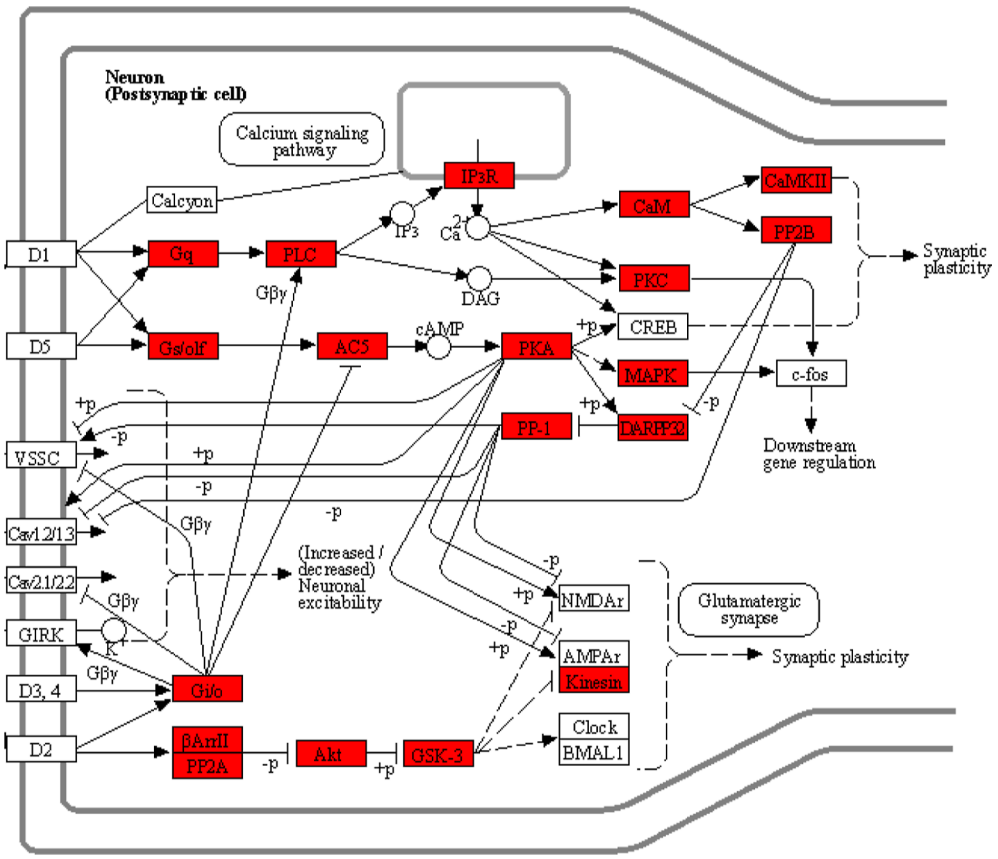

Figure 6. KEGG pathway diagram of dopaminergic synapse with identified proteins from murine brain biopsies punches highlighted in red, produced using ShinyGo[36] and Pathview.[37]

Finally, the hydropathies of identified proteins and peptides in the MCF-7 digest samples were assessed using the GRAVY score to determine whether the surfactants favor hydrophobic or hydrophilic molecules.[50] As shown in Figure S6a, there are minimal differences among Azo, DDM, and the control at the total protein level, likely related to the high overlap in protein identifications. As such, we plotted the same data after excluding the proteins detected in both the Azo- and DDM-containing samples (Figure S6b), revealing that the two surfactants favor the identification of hydrophilic and hydrophobic proteins, respectively. Differences in GRAVY score are more obvious at the peptide level, as shown in Figure S6c, with the DDM-containing samples biased toward more hydrophobic peptides than Azo. The bias is most obvious when the same data are plotted after excluding peptides detected in both the Azo- and DDM-containing samples (Figure S6d), as many more peptides with GRAVY score between −0.5 and 1 are detected in the DDM-containing samples. The observed bias in peptide GRAVY score for the DDM-containing samples aligns with the previous studies reporting high solubilization of hydrophobic membrane peptides in DDM-containing solvents.[48] Notably, to our knowledge, this is the first detailed report demonstrating that the addition of DDM biases the detection of larger and later-eluting peptides.

Overall, these studies suggest that Azo is on par with, if not better than, DDM for microproteomics analysis with orthogonality in peptide identification. Note that in these initial studies, only a single concentration of Azo and DDM was evaluated (for proteomic analysis performance)—of course, we might compare additional concentrations to determine whether the trends described here are universal. Regardless, the results described here suggest that Azo may be a useful new tool for a wide range of microproteome profiling applications in the future. Finally, the DMF method presented here is preliminary, demonstrating a proof-of-concept for Azo-enabled microproteomics analysis. In the future, all of the steps that were implemented manually in this study could be integrated into an end-to-end automated process like the digital microfluidic proteome processing pipeline.[15]

Azo-Enabled DMF Sample Preparation of Mouse Brain Tissue

Having verified the performance of Azo with DMF and LC-MS proteomics performance, we turned to the primary goal of this work—an automated DMF system for processing tissue biopsy samples for proteome profiling. In this work, the heating steps were implemented outside of the DMF control system, and processed samples were collected manually from the devices for injecting into the HPLC-MS. In the future, an "all-in-one" technique[15] might be used, in which integrated thermal control units are used to control the temperature in situ, and processed analytes are automatically delivered from the DMF device to the autosampler of the HPLC-MS system via a custom manifold. Furthermore, it was found that the tissue slices dissolved in the surfactant solutions employed herein. If future studies are carried out with tissue slices that do not completely dissolve, we might consider using hydrophilic surface energy traps[51] to immobilize the samples and/or allow for low-volume extraction.

We hypothesized that the miniaturization of sample preparation on DMF combined with the excellent performance

https://doi.org/10.1021/acs.jproteome.3c00281
J. Proteome Res. 2023, 22, 3242−3253

of Azo would facilitate detailed proteome analysis of microtissue samples without the requirement of specialized techniques like laser capture microdissection. To test this hypothesis, we dissected 2-mm-diameter circular biopsy punches of 10 μm thick tissue slices of murine brain tissue for analysis by a DMF sample preparation workflow. The mass of each tissue biopsy punch was estimated to be approximately 3 μg based on the area of a 10 μm thick tissue slice[52]—this sample size is 2 orders of magnitude smaller than samples evaluated in previous proteomic studies[24−28] implemented with Azo. After processing, the data yielded the identification of 1969 unique protein groups, with an average of 1548 protein groups identified per sample. Protein copy numbers were estimated by normalizing protein intensity to the protein intensities of identified histone proteins, and their distribution is represented in Figure 5a. As shown, high copy number proteins are observed at similar expression levels in all three samples, while lower copy number proteins demonstrate substantial variation in expression across samples. Of the proteins identified in each sample, 56% have coefficient of variation (CV) values under 30%, while 33% of proteins have CV values under 20%. Finally, Figure S7 shows a high degree of reproducibility between the samples tested, demonstrating the reproducibility of this method for microsample analysis.

Among the proteins identified in the murine brain tissue microsamples, cell-specific markers for several cell-types were observed, including (a) astrocytes—GFAP, GSTM1, PRDX6, ALDH1l1, AQP4; (b) oligodendrocytes—MBP, PLP1, MAG, MOG; (c) cerebellar neurons—SNP25, SV2B, GPRIN1, L1CAM, and (d) cortical neurons—ATP1B1, CRMP1, GPM6A, NEFM, NEFL, NEFH.[53] This distribution suggests that the Azo-aided extraction is not biased to a particular cell type. The protein groups that were detected were classified according to the top 20 cellular components that could be assigned based on gene ontology (GO), as shown in Figure 5b. Enrichment relative to baseline levels extrapolated from the protein-coding genome was observed for proteins from the myelin sheath and synaptic regions, similar to what was observed previously in a proteomic study of mouse brain tissue.[54] Among the proteins in this category, there were a number that perform a variety of biological functions from the myelin sheath (such as MYEF2, MBP, MAG, PLP1, MOG, and OMG) and synapse (SYN1, SYN2, SYN3, RIMS1. SYAP1, SYT1, CAMK1D, SNAP25, STX1B),[53] demonstrating the breadth of the proteome identified using the DMF workflow.

The protein groups identified in the murine brain tissue microsamples were then categorized according to the top 100 biological processes that could be assigned based on gene ontology and are displayed in Figure 5c. The majority of identified proteins were found to be involved in transport, organization, biological regulation, and metabolic processes. But more interestingly, a smaller collection of processes related to synaptic signaling and nervous system was observed, which correlates to the synapse processes identified in the GO terms (Figure 5b). To further probe the proteins in these processes, we examined the KEGG pathway for the dopaminergic synapse[38] (Figure 6), highlighting the proteins identified here in red. As shown, high coverage of the KEGG pathway in the postsynaptic neuron was detected from the complex brain tissue sample using the Azo-enabled DMF workflow. In sum, these results demonstrate the capacity for the Azo-enabled DMF proteomics workflow to identify detailed, cell-specific, and pathway-specific markers in minute tissue samples.

CONCLUSIONS

We report the first use of a UV-cleavable surfactant in DMF. The system was applied to develop a workflow for the analysis of tiny (approximately 3 μg) tissue biopsy samples collected from mouse brain slices. A total of 1969 proteins were extracted and identified in these samples, including key cell-type markers associated with a variety of biological functions. We proposed that the combination of Azo with DMF sample preparation is a promising pairing for the automated and sensitive proteomics analysis of size-limited clinical tissue samples using DMF.

ASSOCIATED CONTENT

Supporting Information

The Supporting Information is available free of charge at https://pubs.acs.org/doi/10.1021/acs.jproteome.3c00281.

Degradation of Azo, elution of Azo fragments in LC-MS/MS analysis, elution of DDM in LC-MS/MS analysis, properties of peptides identified in HeLa digest standard, properties of peptides identified in MCF-7 cells, hydrophobicity of peptides and proteins in MCF-7 cells, and Pearson correlation of quantified proteins from tissue biopsies (PDF)

List of peptides from Azo-containing mixtures of protein standard generated from samples after UV irradiation for different periods (XLSX)

Mobility of droplets containing Azo (MP4)

AUTHOR INFORMATION

Corresponding Author

Aaron R. Wheeler − *Department of Chemistry, University of Toronto, Toronto M5S 3H6 Ontario, Canada; Donnelly Centre for Cellular and Biomolecular Research, University of Toronto, Toronto M5S 3E1 Ontario, Canada; Institute of Biomedical Engineering, University of Toronto, Toronto M5S 3G9 Ontario, Canada;* orcid.org/0000-0001-5230-7475; Phone: 416-946-3866; Email: aaron.wheeler@utoronto.ca

Authors

Calvin Chan − *Department of Chemistry, University of Toronto, Toronto M5S 3H6 Ontario, Canada;* orcid.org/0000-0003-0640-0921

Jiaxi Peng − *Department of Chemistry, University of Toronto, Toronto M5S 3H6 Ontario, Canada; Donnelly Centre for Cellular and Biomolecular Research, University of Toronto, Toronto M5S 3E1 Ontario, Canada; Institute of Biomedical Engineering, University of Toronto, Toronto M5S 3G9 Ontario, Canada*

Vigneshwar Rajesh − *Department of Chemistry, University of Toronto, Toronto M5S 3H6 Ontario, Canada;* orcid.org/0000-0001-7436-6943

Erica Y. Scott − *Department of Chemistry, University of Toronto, Toronto M5S 3H6 Ontario, Canada; Donnelly Centre for Cellular and Biomolecular Research, University of Toronto, Toronto M5S 3E1 Ontario, Canada; Institute of Biomedical Engineering, University of Toronto, Toronto M5S 3G9 Ontario, Canada; Department of Surgery, University of Toronto, Toronto M5S 1A8 Ontario, Canada*

Alexandros A. Sklavounos − *Department of Chemistry, University of Toronto, Toronto M5S 3H6 Ontario, Canada; Donnelly Centre for Cellular and Biomolecular Research,*

https://doi.org/10.1021/acs.jproteome.3c00281
J. Proteome Res. 2023, 22, 3242−3253

University of Toronto, Toronto M5S 3E1 Ontario, Canada; orcid.org/0000-0003-1495-7156

Maryam Faiz − *Department of Surgery, University of Toronto, Toronto M5S 1A8 Ontario, Canada*

Complete contact information is available at: https://pubs.acs.org/10.1021/acs.jproteome.3c00281

Author Contributions

C.C., J.P., and A.R.W. conceived the concept of Azo-facilitated proteomics using DMF. C.C., V.R., and A.A.S. performed the surfactant optimization experiments on DMF. C.C. and V.R. characterized the photodegradation of Azo. C.C. and J.P. performed the proteomic experiments on DMF. C.C. and J.P. performed the proteomic data analysis. M.F. and E.Y.S. prepared the tissue samples. C.C., J.P., and A.R.W. wrote and edited the manuscript. All authors discussed the results and commented on the manuscript.

Notes

The authors declare the following competing financial interest(s): A.R.W. is a shareholder in Sci-Bots Inc. (the manufacturer of the DropBot used here).

■ ACKNOWLEDGMENTS

This research was supported by the Canadian Foundation for Innovation (CFI), the Ontario Research Fund (ORF), and the Natural Sciences and Engineering Research Council (NSERC). The authors acknowledge support from Centre for Research and Applications in Fluidic Technologies (CRAFT) for assistance in device fabrication. J.P. acknowledges the Precision Medicine initiative (PRiME) and MITACS postdoctoral fellowships. A.R.W. acknowledges the Canada Research Chairs (CRC) program. Figure 1 and the Table of Contents figure were created with Biorender.com.

■ REFERENCES

(1) Kreitmaier, P.; Katsoula, G.; Zeggini, E. Insights from Multi-Omics Integration in Complex Disease Primary Tissues. *Trends Genet.* **2023**, *39* (1), 46−58.

(2) Akhoundova, D.; Rubin, M. A. Clinical Application of Advanced Multi-Omics Tumor Profiling: Shaping Precision Oncology of the Future. *Cancer Cell* **2022**, *40* (9), 920−938.

(3) Hosp, F.; Mann, M. A Primer on Concepts and Applications of Proteomics in Neuroscience. *Neuron* **2017**, *96* (3), 558−571.

(4) Schmidt, O.; Schulenborg, T.; Meyer, H. E.; Marcus, K.; Hamacher, M. How Proteomics Reveals Potential Biomarkers in Brain Diseases. *Expert Rev. Proteomics* **2005**, *2* (6), 901−913.

(5) Guo, T.; Kouvonen, P.; Koh, C. C.; Gillet, L. C.; Wolski, W. E.; Röst, H. L.; Rosenberger, G.; Collins, B. C.; Blum, L. C.; Gillessen, S.; Joerger, M.; Jochum, W.; Aebersold, R. Rapid Mass Spectrometric Conversion of Tissue Biopsy Samples into Permanent Quantitative Digital Proteome Maps. *Nat. Med.* **2015**, *21* (4), 407−413.

(6) Alexovič, M.; Sabo, J.; Longuespée, R. Microproteomic Sample Preparation. *Proteomics* **2021**, *21* (9), 2000318.

(7) Feist, P.; Hummon, A. B. Proteomic Challenges: Sample Preparation Techniques for Microgram-Quantity Protein Analysis from Biological Samples. *Int. J. Mol. Sci.* **2015**, *16* (2), 3537−3563.

(8) Ethier, M.; Hou, W.; Duewel, H. S.; Figeys, D. The Proteomic Reactor: A Microfluidic Device for Processing Minute Amounts of Protein Prior to Mass Spectrometry Analysis. *J. Proteome Res.* **2006**, *5* (10), 2754−2759.

(9) Li, Z. Y.; Huang, M.; Wang, X.-K.; Zhu, Y.; Li, J.-S.; Wong, C. C. L.; Fang, Q. Nanoliter-Scale Oil-Air-Droplet Chip-Based Single Cell Proteomic Analysis. *Anal. Chem.* **2018**, *90* (8), 5430−5438.

(10) Liang, Y.; Acor, H.; McCown, M. A.; Nwosu, A. J.; Boekweg, H.; Axtell, N. B.; Truong, T.; Cong, Y.; Payne, S. H.; Kelly, R. T. Fully Automated Sample Processing and Analysis Workflow for Low-Input Proteome Profiling. *Anal. Chem.* **2021**, *93* (3), 1658−1666.

(11) Mousa, N. A.; Jebrail, M. J.; Yang, H.; Abdelgawad, M.; Metalnikov, P.; Chen, J.; Wheeler, A. R.; Casper, R. F. Droplet-Scale Estrogen Assays in Breast Tissue, Blood, and Serum. *Sci. Transl. Med.* **2009**, *1* (1), 1ra2.

(12) Kim, J.; Abdulwahab, S.; Choi, K.; Lafrenière, N. M.; Mudrik, J. M.; Gomaa, H.; Ahmado, H.; Behan, L.-A.; Casper, R. F.; Wheeler, A. R. A Microfluidic Technique for Quantification of Steroids in Core Needle Biopsies. *Anal. Chem.* **2015**, *87* (9), 4688−4695.

(13) Abdulwahab, S.; Ng, A. H. C.; Chamberlain, M. D.; Ahmado, H.; Behan, L.-A.; Gomaa, H.; Casper, R. F.; Wheeler, A. R. Towards a Personalized Approach to Aromatase Inhibitor Therapy: A Digital Microfluidic Platform for Rapid Analysis of Estradiol in Core-Needle-Biopsies. *Lab Chip* **2017**, *17* (9), 1594−1602.

(14) Huang, Y.; Williams, J. C.; Johnson, S. M. Brain Slice on a Chip: Opportunities and Challenges of Applying Microfluidic Technology to Intact Tissues. *Lab Chip* **2012**, *12* (12), 2103−2117.

(15) Peng, J.; Chan, C.; Zhang, S.; Sklavounos, A. A.; Olson, M. E.; Scott, E. Y.; Hu, Y.; Rajesh, V.; Li, B. B.; Chamberlain, M. D.; Zhang, S.; Peng, H.; Wheeler, A. R. All-in-One Digital Microfluidics Pipeline for Proteomic Sample Preparation and Analysis. *Chem. Sci.* **2023**, *14* (11), 2887−2900.

(16) Steinbach, M. K.; Leipert, J.; Blurton, C.; Leippe, M.; Tholey, A. Digital Microfluidics Supported Microproteomics for Quantitative Proteome Analysis of Single Caenorhabditis Elegans Nematodes. *J. Proteome Res.* **2022**, *21* (8), 1986−1996.

(17) Luk, V. N.; Mo, G. C. H.; Wheeler, A. R. Pluronic Additives: A Solution to Sticky Problems in Digital Microfluidics. *Langmuir* **2008**, *24* (12), 6382−6389.

(18) Au, S. H.; Kumar, P.; Wheeler, A. R. A New Angle on Pluronic Additives: Advancing Droplets and Understanding in Digital Microfluidics. *Langmuir* **2011**, *27* (13), 8586−8594.

(19) Ho, M.; Au, A.; Flick, R.; Vuong, T. V.; Sklavounos, A. A.; Swyer, I.; Yip, C. M.; Wheeler, A. R. Anti-Fouling Properties of Pluronic and Tetronic Surfactants in Digital Microfluidics. *ACS Appl. Mater. Interfaces* **2023**, *15* (5), 6326−6337.

(20) Lamanna, J.; Scott, E. Y.; Edwards, H. S.; Chamberlain, M. D.; Dryden, M. D. M.; Peng, J.; Mair, B.; Lee, A.; Chan, C.; Sklavounos, A. A.; Heffernan, A.; Abbas, F.; Lam, C.; Olson, M. E.; Moffat, J.; Wheeler, A. R. Digital Microfluidic Isolation of Single Cells for -Omics. *Nat. Commun.* **2020**, *11* (1), 5632.

(21) Leipert, J.; Tholey, A. Miniaturized Sample Preparation on a Digital Microfluidics Device for Sensitive Bottom-up Microproteomics of Mammalian Cells Using Magnetic Beads and Mass Spectrometry-Compatible Surfactants. *Lab Chip* **2019**, *19* (20), 3490−3498.

(22) Leipert, J.; Steinbach, M. K.; Tholey, A. Isobaric Peptide Labeling on Digital Microfluidics for Quantitative Low Cell Number Proteomics. *Anal. Chem.* **2021**, *93* (15), 6278−6286.

(23) Leipert, J.; Kaulich, P. T.; Steinbach, M. K.; Steer, B.; Winkels, K.; Blurton, C.; Leippe, M.; Tholey, A. Digital Microfluidics and Magnetic Bead-Based Intact Proteoform Elution for Quantitative Top-down Nanoproteomics of Single *C.elegans* Nematodes. *Angew. Chem., Int. Ed.* **2023**, *62*, No. e202301969.

(24) Brown, K. A.; Chen, B.; Guardado-Alvarez, T. M.; Lin, Z.; Hwang, L.; Ayaz-Guner, S.; Jin, S.; Ge, Y. A Photocleavable Surfactant for Top-down Proteomics. *Nat. Methods* **2019**, *16* (5), 417−420.

(25) Brown, K. A.; Tucholski, T.; Eken, C.; Knott, S.; Zhu, Y.; Jin, S.; Ge, Y. High-Throughput Proteomics Enabled by a Photocleavable Surfactant. *Angew. Chem., Int. Ed.* **2020**, *59* (22), 8406−8410.

(26) Knott, S. J.; Brown, K. A.; Josyer, H.; Carr, A.; Inman, D.; Jin, S.; Friedl, A.; Ponik, S. M.; Ge, Y. Photocleavable Surfactant-Enabled Extracellular Matrix Proteomics. *Anal. Chem.* **2020**, *92* (24), 15693−15698.

(27) Aballo, T. J.; Roberts, D. S.; Melby, J. A.; Buck, K. M.; Brown, K. A.; Ge, Y. Ultrafast and Reproducible Proteomics from Small

Amounts of Heart Tissue Enabled by Azo and TimsTOF Pro. *J. Proteome Res.* **2021**, *20* (8), 4203−4211.
(28) Buck, K. M.; Roberts, D. S.; Aballo, T. J.; Inman, D. R.; Jin, S.; Ponik, S.; Brown, K. A.; Ge, Y. One-Pot Exosome Proteomics Enabled by a Photocleavable Surfactant. *Anal. Chem.* **2022**, *94* (20), 7164−7168.
(29) Fobel, R.; Fobel, C.; Wheeler, A. R. DropBot: An Open-Source Digital Microfluidic Control System with Precise Control of Electrostatic Driving Force and Instantaneous Drop Velocity Measurement. *Appl. Phys. Lett.* **2013**, *102* (19), 193513.
(30) Swyer, I.; Fobel, R.; Wheeler, A. R. Velocity Saturation in Digital Microfluidics. *Langmuir* **2019**, *35* (15), 5342−5352.
(31) Tyanova, S.; Temu, T.; Cox, J. The MaxQuant Computational Platform for Mass Spectrometry-Based Shotgun Proteomics. *Nat. Protoc.* **2016**, *11* (12), 2301−2319.
(32) Tyanova, S.; Temu, T.; Sinitcyn, P.; Carlson, A.; Hein, M. Y.; Geiger, T.; Mann, M.; Cox, J. The Perseus Computational Platform for Comprehensive Analysis of (Prote)Omics Data. *Nat. Methods* **2016**, *13* (9), 731−740.
(33) Wiśniewski, J. R.; Hein, M. Y.; Cox, J.; Mann, M. A "Proteomic Ruler" for Protein Copy Number and Concentration Estimation without Spike-in Standards. *Mol. Cell. Proteomics* **2014**, *13* (12), 3497−3506.
(34) Stothard, P. The Sequence Manipulation Suite: JavaScript Programs for Analyzing and Formatting Protein and DNA Sequences. *BioTechniques* **2000**, *28*, 1102−1104.
(35) *OriginPro* (v. 2021b); OriginLab Corp.: Northampton, MA, USA, 2021. http://www.originlab.com.
(36) Ge, S. X.; Jung, D.; Yao, R. ShinyGO: A Graphical Gene-Set Enrichment Tool for Animals and Plants. *Bioinformatics* **2020**, *36* (8), 2628−2629.
(37) Luo, W.; Brouwer, C. Pathview: An R/Bioconductor Package for Pathway-Based Data Integration and Visualization. *Bioinformatics* **2013**, *29* (14), 1830−1831.
(38) Kanehisa, M.; Furumichi, M.; Sato, Y.; Ishiguro-Watanabe, M.; Tanabe, M. KEGG: Integrating Viruses and Cellular Organisms. *Nucleic Acids Res.* **2021**, *49* (D1), D545−D551.
(39) Mi, H.; Huang, X.; Muruganujan, A.; Tang, H.; Mills, C.; Kang, D.; Thomas, P. D. PANTHER Version 11: Expanded Annotation Data from Gene Ontology and Reactome Pathways, and Data Analysis Tool Enhancements. *Nucleic Acids Res.* **2017**, *45* (D1), D183−D189.
(40) Supek, F.; Bošnjak, M.; Škunca, N.; Šmuc, T. REVIGO Summarizes and Visualizes Long Lists of Gene Ontology Terms. *PLoS One* **2011**, *6* (7), No. e21800.
(41) Shannon, P.; Markiel, A.; Ozier, O.; Baliga, N. S.; Wang, J. T.; Ramage, D.; Amin, N.; Schwikowski, B.; Ideker, T. Cytoscape: A Software Environment for Integrated Models of Biomolecular Interaction Networks. *Genome Res.* **2003**, *13* (11), 2498−2504.
(42) Perez-Riverol, Y.; Csordas, A.; Bai, J.; Bernal-Llinares, M.; Hewapathirana, S.; Kundu, D. J.; Inuganti, A.; Griss, J.; Mayer, G.; Eisenacher, M.; Pérez, E.; Uszkoreit, J.; Pfeuffer, J.; Sachsenberg, T.; Yılmaz, Ş.; Tiwary, S.; Cox, J.; Audain, E.; Walzer, M.; Jarnuczak, A. F.; Ternent, T.; Brazma, A.; Vizcaíno, J. A. The PRIDE Database and Related Tools and Resources in 2019: Improving Support for Quantification Data. *Nucleic Acids Res.* **2019**, *47* (D1), D442−D450.
(43) Dou, M.; Clair, G.; Tsai, C.-F.; Xu, K.; Chrisler, W. B.; Sontag, R. L.; Zhao, R.; Moore, R. J.; Liu, T.; Pasa-Tolic, L.; Smith, R. D.; Shi, T.; Adkins, J. N.; Qian, W.-J.; Kelly, R. T.; Ansong, C.; Zhu, Y. High-Throughput Single Cell Proteomics Enabled by Multiplex Isobaric Labeling in a Nanodroplet Sample Preparation Platform. *Anal. Chem.* **2019**, *91* (20), 13119−13127.
(44) Tsai, C.-F.; Zhang, P.; Scholten, D.; Martin, K.; Wang, Y.-T.; Zhao, R.; Chrisler, W. B.; Patel, D. B.; Dou, M.; Jia, Y.; Reduzzi, C.; Liu, X.; Moore, R. J.; Burnum-Johnson, K. E.; Lin, M.-H.; Hsu, C.-C.; Jacobs, J. M.; Kagan, J.; Srivastava, S.; Rodland, K. D.; Steven Wiley, H.; Qian, W.-J.; Smith, R. D.; Zhu, Y.; Cristofanilli, M.; Liu, T.; Liu, H.; Shi, T. Surfactant-Assisted One-Pot Sample Preparation for Label-Free Single-Cell Proteomics. *Commun. Biol.* **2021**, *4* (1), 265−312.
(45) Kwon, Y.; Piehowski, P. D.; Zhao, R.; Sontag, R. L.; Moore, R. J.; Burnum-Johnson, K. E.; Smith, R. D.; Qian, W.-J.; Kelly, R. T.; Zhu, Y. Hanging Drop Sample Preparation Improves Sensitivity of Spatial Proteomics. *Lab Chip* **2022**, *22* (15), 2869−2877.
(46) Proc, J. L.; Kuzyk, M. A.; Hardie, D. B.; Yang, J.; Smith, D. S.; Jackson, A. M.; Parker, C. E.; Borchers, C. H. A Quantitative Study of the Effects of Chaotropic Agents, Surfactants, and Solvents on the Digestion Efficiency of Human Plasma Proteins by Trypsin. *J. Proteome Res.* **2010**, *9* (10), 5422−5437.
(47) Dunkin, I. R.; Gittinger, A.; Sherrington, D. C.; Whittaker, P. Synthesis, Characterization and Applications of Azo-Containing Photodestructible Surfactants. *J. Chem. Soc., Perkin Trans. 2* **1996**, No. 9, 1837−1842.
(48) Zhang, X. Less Is More: Membrane Protein Digestion Beyond Urea-Trypsin Solution for Next-Level Proteomics. *Mol. Cell. Proteomics* **2015**, *14* (9), 2441−2453.
(49) Liu, J.; Wang, F.; Mao, J.; Zhang, Z.; Liu, Z.; Huang, G.; Cheng, K.; Zou, H. High-Sensitivity N-Glycoproteomic Analysis of Mouse Brain Tissue by Protein Extraction with a Mild Detergent of N-Dodecyl *β*-D-Maltoside. *Anal. Chem.* **2015**, *87* (4), 2054−2057.
(50) Kyte, J.; Doolittle, R. F. A Simple Method for Displaying the Hydropathic Character of a Protein. *J. Mol. Bio.* **1982**, *157* (1), 105−132.
(51) McEwen, R. A. H.; Hermann, M.; Metwally, H.; Donovan, K.; Liu, C.; Le Blanc, J. C. Y.; Covey, T. R.; Oleschuk, R. Discontinuously Dewetting Solvent Arrays: Droplet Formation and Poly-Synchronous Surface Extraction for Mass Spectrometry Imaging Applications. *Anal. Chem.* **2022**, *94* (20), 7219−7228.
(52) de Graaf, E. L.; Pellegrini, D.; McDonnell, L. A. Set of Novel Automated Quantitative Microproteomics Protocols for Small Sample Amounts and Its Application to Kidney Tissue Substructures. *J. Proteome Res.* **2016**, *15* (12), 4722−4730.
(53) Korovesi, A. G.; Anagnostopoulos, A. K.; Pierros, V.; Stravopodis, D. J.; Tsangaris, G. T. Normal Mouse Brain Proteome II: Analysis of Brain Regions by High-Resolution Mass Spectrometry. *Cancer Genomics Proteomics* **2020**, *17* (6), 757−767.
(54) Sharma, K.; Schmitt, S.; Bergner, C. G.; Tyanova, S.; Kannaiyan, N.; Manrique-Hoyos, N.; Kongi, K.; Cantuti, L.; Hanisch, U.-K.; Philips, M.-A.; Rossner, M. J.; Mann, M.; Simons, M. Cell Type- and Brain Region-Resolved Mouse Brain Proteome. *Nat. Neurosci.* **2015**, *18* (12), 1819−1831.

https://doi.org/10.1021/acs.jproteome.3c00281
J. Proteome Res. 2023, 22, 3242−3253